J. exp. Biol. **166**, 145–168 (1992)
Printed in Great Britain © *The Company of Biologists Limited 1992*

SURFACE STRAIN ON THE EQUINE HOOF WALL *IN VIVO*: IMPLICATIONS FOR THE MATERIAL DESIGN AND FUNCTIONAL MORPHOLOGY OF THE WALL

BY J. J. THOMASON

Department of Zoological and Biomedical Sciences and College of Osteopathic Medicine, Ohio University, Athens, OH 45701, USA

A. A. BIEWENER

Department of Organismal Biology and Anatomy, The University of Chicago, Chicago, IL 60637, USA

AND J. E. A. BERTRAM

Concord Field Station, Harvard University, Bedford, MA 01730, USA

Accepted 17 January 1992

Summary

Surface strains were recorded from four rosette gauges at different sites on the right forehooves of three ponies running on a treadmill at seven constant speeds and using three gaits. Principal strains determined from the rosette signals indicate that the hoof material is loaded predominantly in compression and that the wall is distorted in a regular, repeatable manner at all speeds and gaits. Peak principal strains reach $-5000\,\mu\epsilon$, compared with $-2800\,\mu\epsilon$ reported for the equine radius under similar locomotory conditions. Orientations of peak compressive strains do not correlate strongly with microstructural axes in the material. Comparison of our *in vivo* strain records with previous *in vitro* studies of the material properties of the wall shows that hoof keratin behaves as a multidirectional composite, capable of tolerating its usual operating strains in any direction. This mechanical behaviour also allows the material to withstand many unpredictable loading situations when the hoof contacts irregular substrata. An important property of the hoof wall is its ability to resist or redirect cracks. We found that the anterior aspect of the wall is loaded in biaxial compression, which assists in preventing the formation or propagation of cracks and reduces peak strain magnitudes. The strain patterns correlate well with current models of hoof distortion during weight-bearing. In these models, transmission of force between the ground and the skeleton is seen as the primary cause of compression in the material. The third phalanx, which transmits the weight, is effectively suspended from the inner surface of the hoof wall. Spreading of the posterior borders (heels) of the hoof also occurs. The combination of weight-bearing, suspension of the third phalanx and heel spreading is probably responsible for the uncommon loading condition of biaxial compression on the anterior wall.

Key words: strain, horse hoof, keratin, material design, functional morphology, locomotion, adaptation.

Introduction

Our aim in this paper is to link current interpretations of the functional design of hoof material, which were derived from histological studies and engineering tests *in vitro*, with an assessment of how the material is loaded *in vivo*. Investigations of the forces acting on the hoof *in vivo* date back to the last century. Lungwitz (1891, cited in Colles, 1989*a*) used electrical contacts to detect relative motion of the various parts of the hoof wall. More recently, electrical strain gauges have been used on the outer surface of the wall by a number of workers (Knezevic, 1962; Preuschoft, 1989; Zoerb and Leach, 1978; Colles, 1989*a*,*b*; Mair, 1974). All of these studies addressed questions of veterinary significance – on overall distortion of the hoof, the contribution of parts other than the wall to weight-bearing, or comparisons of normal and pathologically distorted hooves – and none provides the link we seek.

The key question we address is whether the peak principal strains developed in the material during locomotion correspond to the anisotropic mechanical properties conferred by its architecture. Most of the studies on hoof strain cited above used single-element gauges, which do not give the magnitudes or orientations of the principal tensile and compressive strains in the material. To obtain this information we used rosette strain gauges placed at four sites around the circumference of the hoof. The sites were selected on the basis of the previous veterinary studies and also allow us to address the question of how forces are transmitted to and through the wall.

The following sections introduce current functional interpretations of the microscopic and gross structure of the hoof wall for comparison with our results.

The microstructure and material properties of the hoof wall

The material of the equine hoof wall is highly oriented under the light microscope (Stump, 1967; Leach, 1980). Half of the thickest layer of the wall, the *stratum medium* (Fig. 1B: SM), consists of tubules running proximodistally, parallel to the surface (Fig. 1A: T). The other half of the layer is intertubular material, which is arranged tangentially around the circumference of the hoof (Fig. 1A: I). At the front of the hoof, the tubules and intertubular material intersect orthogonally, while the angle of intersection reduces to 45–65° at the sides of the hoof.

This strong microscopic alignment is reflected in the anisotropic physical properties of the hoof wall. However, the most obvious properties to study – strength and stiffness – are anisotropic in ways that are difficult to interpret in terms of the probable loading of the material. Leach (1980) assumed that, during weight-bearing, much of the ground reaction force is transmitted proximally up the wall, i.e. parallel to the tubules. But he found that the compressive stiffness of samples from the anterior wall was 50–80 % higher perpendicular to the tubules than parallel to them. The material is stiffer normal to the direction in which intuition tells us it is probably loaded. The results of tensile experiments were

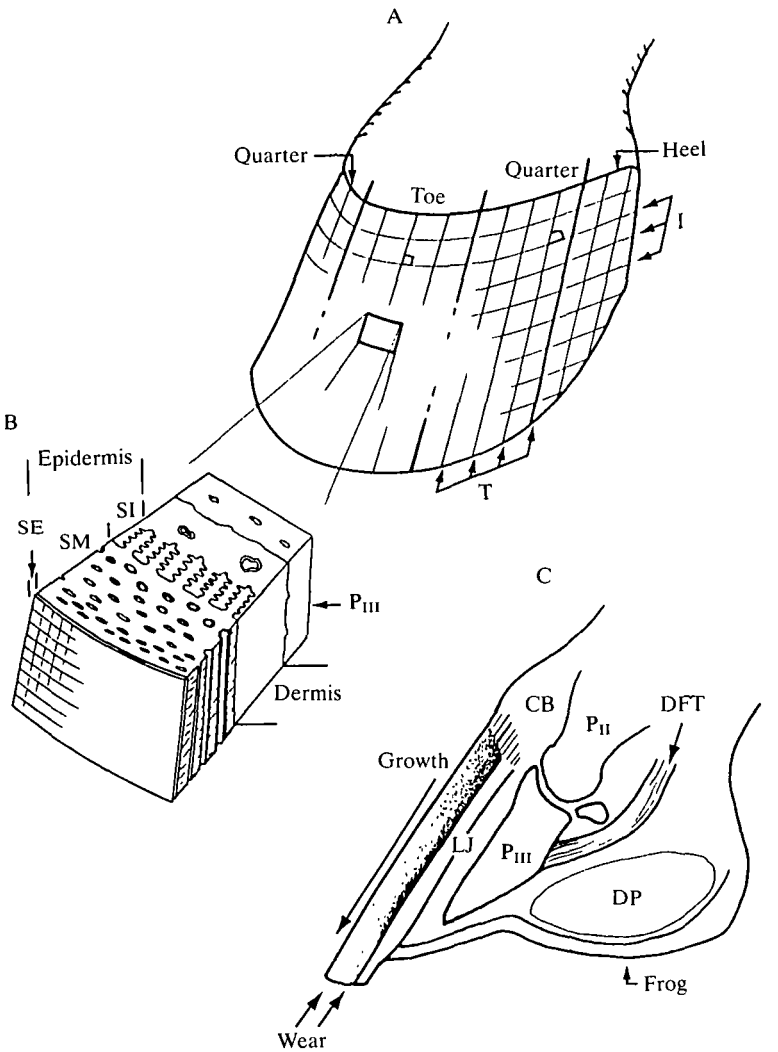

Fig. 1. Morphology of the equine hoof. (A) Regions of the wall, and the orientation of tubules (T) and intertubular material (I). (B) Enlargement of a block removed from the toe showing the layers of the wall (redrawn after Stump, 1967). SE, SM and SI are the *strata externum*, *medium* and *internum*, respectively. (C) Sagittal section through the hoof. Stippling represents the gradients of relative hydration in the *stratum medium* (redrawn after Bertram and Gosline, 1987). CB, coronary border; DFT, deep digital flexor tendon; DP, digital pad; LJ, lamellar junction; P_{II} and P_{III}, second and third phalanges of the third digit.

similarly enigmatic at first sight. Tensile strength and stiffness are also greater parallel to the intertubular material than parallel to the tubules, by 22 % and 15 %, respectively (Bertram and Gosline, 1986). As we discuss below, the variation in tensile stiffness with hydration level may be more important than its anisotropy.

These results emphasize that, while the material appears to be reinforced by the tubules, the intertubular material accounts for much of its mechanical behaviour (Leach, 1980).

Leach (1980) observed that compressive stiffness varied with hydration level and discussed the probable effects on the energy-absorbing capability of the material that such variation implies. Later, Bertram and Gosline (1986) showed that energy absorption may indeed be more a important factor than static strength in the functional design of the hoof wall. In their *in vitro* study, one measure of energy absorption was quantified as the fracture toughness (which indicates a material's resistance to the formation and spreading of cracks). For notched specimens of hoof wall under tensile load, cracks always propagated in the intertubular direction, fracturing the tubules, even if the notch was itself aligned with the tubules (Bertram and Gosline, 1986). Again, the intertubular material has the greater reinforcing effect. This finding has important functional significance. Cracks starting at the free margin of the hoof in the living animal will tend not to run up through the wall, but will usually turn, harmlessly, parallel to the edge. Losing slivers of material by fracture at the distal margin is part of the normal wear process. Although the hoof wall is dead material, it is continuously generated, as are most epidermal tissues and derivatives, from a basement membrane located in this case at the coronary border (Fig. 1C: CB). The proximodistal direction of growth is directly opposite to the direction of wear.

Unlike bone, which is continually remodelled, the microscopic architecture of hoof keratin is fixed once the generative cells die and derives from the topology of the basement membrane (Stump, 1967; Leach, 1980). Intertubular material is formed from flattened cells (keratinocytes) oriented parallel to the surface of the membrane. Keratinocytes forming the tubules grow around slender papillae projecting from the plane of the membrane. Once cells are a few layers removed from the membrane they shrink and die. The keratin fibrils and amorphous protein matrix which comprise most of their contents form inter- and intramolecular disulphide crosslinks (Fraser and MacRae, 1980). Annular gap junctions between the cells are also important in linking the contents of adjacent cells (Leach and Oliphant, 1984). The result is a mechanically stable, multidirectional, fibre-reinforced composite (Bertram and Gosline, 1986). (The orientation of keratin fibres differs between tubules and intertubular material and between tubules at different depths. These molecular orientations undoubtedly contribute to the composite nature of the material, but such effects are out of our purview.)

Although the microscopic structure of hoof keratin is fixed, its material properties vary with relative hydration (Leach, 1980; Bertram and Gosline, 1987). Two gradients of relative hydration exist in the wall (Fig. 1C: stippling). One parallels the growth direction: it is high at the coronary border, where the keratinocytes are alive, and low at the distal margin. The other gradient is high on the inside of the wall, where moisture is replenished from the vascularized dermis. It is low at the outside surface because moisture is lost to the air, though the thin, lipid-rich *stratum externum* (Fig. 1B: SE) provides some waterproofing (Leach,

1980). The main effect of the hydration gradients is that most of the hoof wall is operating nearly at maximum fracture toughness. Fracture toughness is maximal in the region of 75 % relative hydration, which is in the centre of the range of hydration levels found through most of the *stratum medium* (Bertram and Gosline, 1987). At this level of hydration the stress–strain curve for tensile loading has a long plastic region before failure (Bertram and Gosline, 1987), giving the material high energy-absorbing capacity.

The relative hydration of the *stratum medium* increases to 100 % towards the inner layer of the epidermis, the *stratum internum* (Fig. 1B: SI). The effect is to reduce the fracture toughness and also the tensile stiffness. The *stratum internum* has an even lower stiffness, owing to a lower degree of keratinization than the *stratum medium*. This gradient of reducing stiffness, partly mediated by hydration levels, has been interpreted as a mechanism to smooth energy transfer between the wall and the living cells of the underlying dermis (Leach, 1980; Bertram and Gosline, 1987).

Close to the distal margin, hydration levels drop rapidly and fracture toughness falls to roughly 25 % of maximum. However, tensile stiffness varies inversely with relative hydration, with a greater increase on drying than in other keratins that have been studied. The tensile strength of hoof keratin at 0 % relative humidity is 35 times higher than at 100 % (Bertram and Gosline, 1987), compared with a factor of 3 for both horsehair and wool (Fraser and MacCrae, 1980). Bertram and Gosline (1987) were cautious in interpreting the large change in stiffness on drying in hoof keratin, but suggested that it may be accompanied by an increase in abrasion resistance towards the part of the wall making contact with the ground.

Hoof morphology and the forces acting on the wall

The hoof wall is an obliquely truncated cone that opens posteriorly between the heels (Figs 1A, 2D). The wall has to withstand two types of loading: high-velocity impacts with the ground and transmission of forces between the ground and the skeleton.

Force transmission is generally modelled in the sagittal plane for simplicity (Leach, 1980; Bartel *et al.* 1978). The ground reaction forces (Fig. 2A: **g**) distributed over the hoof wall during weight-bearing may be resolved as a single vector **G**. At its peak magnitude, **G** is vertically oriented and acts through the mid-point of the hoof (Bartel *et al.* 1978). It counteracts the downward force of the body (**W**), transmitted through the third phalanx (P_{III}).

Physical separation of the wall and P_{III} is resisted by a complex lamellar junction (Fig. 1C: LJ). The deepest layer of the wall, the *stratum internum* (or *stratum lamellum*, Fig. 1B: SI), forms a series of primary and secondary lamellae which greatly increase its area of contact with the dermis (Stump, 1967). They interlock with living, well-vascularized lamellae of the dermis (Fig. 1B), which is bound to the periosteum of P_{III}. The distal migration of the wall as it grows is accomplished by the epidermal lamellae sliding past those of the dermis.

Because the wall is oblique to the direction of the ground reaction forces **g**, these

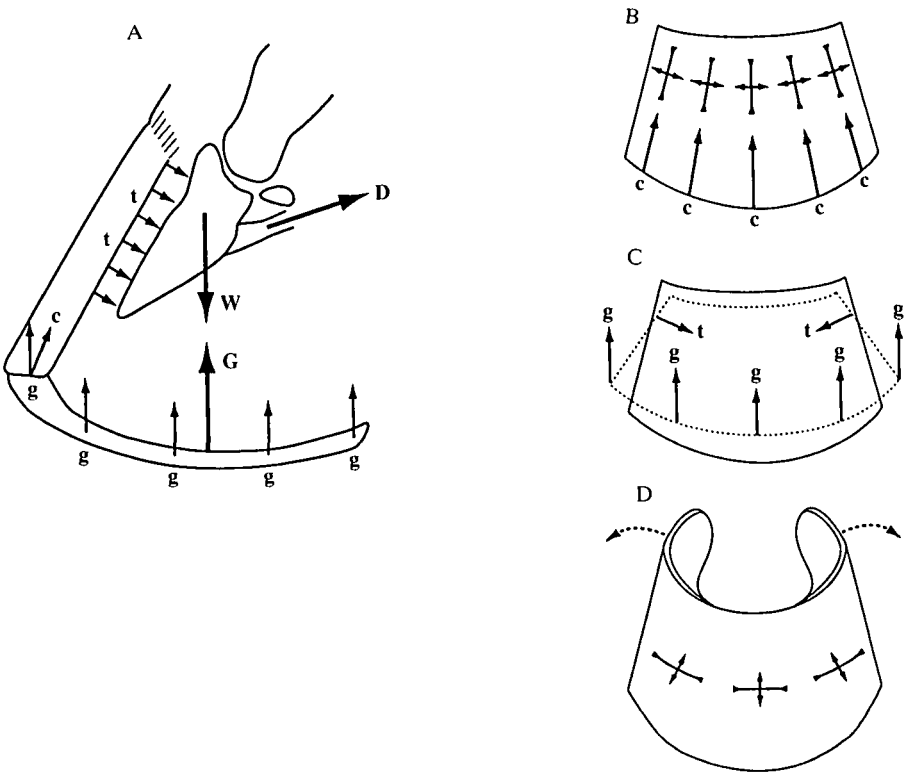

Fig. 2. Loading of the hoof wall. (A) Transmission of forces between the wall and the skeleton in sagittal section. Vectors **g** are components of the resultant ground reaction force **G** distributed around the distal margin of the wall. Other forces are described in the text, and only forces or components that are discussed in the text are shown. No attempt has been made to balance the forces acting on each structure. (B) Compressive forces **c** in the wall in anterior view and the strains they are likely to induce. (C) The effect of inwardly directed tensile forces **t** and components of ground reaction force **g**, in anterior view. (D) Spreading of the heels, and the strains it might induce. **W**, downward force of the body; **D**, tensile force in the deep digital flexor tendon.

must have compressive components (Fig. 2A: **c**) parallel to the wall and inwardly directed tensile components (Fig. 2A: **t**). Components **c** are primarily resisted by the wall, components **t** by the lamellar junction; 'consequently the wall suspends the weight of the horse' (Leach, 1980; p.199). The large area of contact, owing to the lamellar folding, helps reduce stresses acting on the living dermal cells to tolerable levels (Stump, 1967). As noted above, the compliance of the *stratum internum* probably evens out energy transfer between wall and dermis (Leach, 1980; Bertram and Gosline, 1987).

In the sagittal plane, forces **t** cause posteroventral movement of both P_{III} and the anterior wall by an amount that is visible in lateral radiographs of statically loaded hooves (Fischerleitner, 1974). That the bone and wall move by nearly equal amounts attests to the strength of the lamellar junction. In an *in vitro* test of a

block such as that shown in Fig. 1B the periosteum separated from P_{III} before the lamellar junction failed (J. E. A. Bertram, unpublished results).

The magnitudes of components **t** are increased by a large tensile force (Fig. 2A: **D**) in the deep digital flexor tendon (Fig. 1C: DFT), exerting torque on P_{III} about P_{II}. This torque tends to rotate the anterior border of P_{III} ventrally. The existence of the torque is dramatically illustrated in extreme cases of laminitis (inflammation of the living dermal lamellae) when the lamellar junction fails and the anterior border of P_{III} may penetrate the sole (Coffman *et al.* 1970).

While the sagittal view illustrates the major forces transmitted by the wall, loading in other planes cannot be ignored (Leach, 1980). In three dimensions, components **c** are distributed around the circumference of the wall (Fig. 2B). They act parallel to the tubules at the toe, but are oblique to both tubules and intertubular material at the heels and quarters. These components will induce compressive strains in the wall, parallel to the forces, with smaller perpendicular tensile strains as the material tends to maintain its volume.

Components of **t** induce a complex three-dimensional distortion of the hoof. The lamellar junction is widest at the toe and quarters, but narrows rapidly towards the heels (Getty, 1975). Components **t** are, therefore, mostly confined to the anterior half of the hoof. In anterior view (Fig. 2C), components **t** at the quarters pull inwards and downwards on the wall. This action is confirmed by the observation of Lungwitz (1891, cited in Colles, 1989*a*) that the anterior half of the coronary band constricts during weight-bearing. We might expect constriction at the coronary band to be accompanied by expansion at the distal margin caused by components of the ground reaction force (Fig. 2C). Such distortion would cause torsion at the quarters and, therefore, high levels of shear strain. The effect of these distortions on principal compressive and tensile strains recorded at the surface is difficult to predict.

The final contribution to loading of the wall that we will discuss is spreading of the heels during weight-bearing, observed by Lungwitz (1891, cited in Colles, 1989*a*). Colles (1989*a*) confirmed the occurrence of heel spreading using single foil gauges. This action has two probable and combinatory causes. First, as weight is put on the leg, the digit rotates ventrally about the P_{II}–P_{III} joint. Downward rotation of P_{II} compresses a fatty, resilient digital pad (Fig. 1C: DP) and probably forces apart the lateral cartilages (not shown) which extend posteriorly from P_{III} to either side of P_{II}. The compressed digital pad expands laterally, exerting pressure on the heels, while movement of the lateral cartilages will be transmitted directly to the heels. Second, the frog, a keratinized structure connected to the sole (Fig. 1C), may contact the ground, and upward force on the frog will help compress the digital pad. Motion of the frog is also probably transmitted directly to the heels by other features of the sole known as the bars (not shown). The contribution of the frog to weight-bearing is a subject of continuing debate in the veterinary literature (Colles, 1989*a*).

If the wall were equally thick and rigid around its circumference, spreading of the heels would induce horizontally oriented compressive strain at the toe and

quarters (Fig. 2D). This strain is perpendicular to the compression induced by components of **g** (Fig. 2B). Strain gauges at the toe indicate that such biaxial compression does occur (Mair, 1974; J. J. Thomason, A. P. Russell and S. Hunt, unpublished results). The finding is a little surprising because the heels are considerably thinner and more flexible than the anterior part of the wall (Leach, 1980) and may be deformed locally without major deformation at the toe. Indeed, the heels still spread when motion of the anterior two-thirds of the wall is constrained by a shoe (Colles, 1989*a*). We shall return to this point in the Discussion.

A major reason why loading of the wall has proved difficult to quantify is that gauges may be attached only to its outer surface. To determine how strain patterns change through the wall it would be necessary to have gauges on its inner surface. While it is possible surgically to implant strain gauges on bones *in vivo* (e.g. Biewener *et al.* 1983), gaining surgical access to the inside of the hoof wall would destroy the lamellar junction and, hence, the functional integrity of the hoof. The application of rosette gauges to the hoof surface will help unravel some of the complex loading patterns described above, but still will not give a complete picture. Another limitation lies in the restricted range of material properties that have been measured to date. To calculate principal stresses for an anisotropic material, Poisson's ratios and shear moduli must be known in addition to compressive and tensile elastic moduli (Carter, 1978). Only the Young's moduli are available for hoof wall.

Materials and methods

Three small ponies (body masses 165–175 kg) were trained to run on a treadmill until they changed gaits at consistent speeds. They were unshod, and the hooves were field trimmed (i.e. clipped and filed evenly to compensate for reduced wear on a soft substratum). Rosette strain gauges were attached with cyanoacrylate adhesive at four sites on the right front hoof of each animal. Colles (1989*b*) describes the techniques for the preparation and cleaning of the wall and for gauge attachment. (Gauge sites are illustrated, with some resulting principal strains, in Fig. 5.) Two gauges were placed one above the other at the toe (anterior midline), approximately one-quarter and three-quarters of the way down the wall. These proximal anterior (PA) and distal anterior (DA) gauges were on, or close to, the morphological midline axis of the hoof. Their output allowed us to assess (1) the magnitudes of the peak principal strains in the material, (2) the orientation of the peak principal strains with respect to the tubules and orthogonal intertubular material, (3) whether the toe is subjected to biaxial compression, and (4) whether tubules experienced similar loading patterns along their length. Rosette gauges were also placed on lateral (L) and medial (M) quarters, approximately half way up the wall. These gauges gave strain magnitudes and orientation at sites where the tubular and intertubular material were not orthogonal. They also indicated the extent to which movement at the heels results in strain at the toe, because the

effects of such movement have to be transmitted *via* the quarters. We use the abbreviations PA, DA, L and M with the postfixed numbers 1, 2 and 3 to refer to the gauges on each animal.

Each gauge was photographed perpendicular to its plane so that we could determine its orientation with respect to the architecture of the hoof wall. The orientation of tubules and intertubular material is represented by surface striations. The angles between the axis of each rosette and both sets of striations were measured to the nearest 5°.

The horses were run at seven speeds through three gaits: walk (1 and 1.5 $m\,s^{-1}$), trot (2, 3 and 3.75 $m\,s^{-1}$) and canter/gallop (4.5 and 6 $m\,s^{-1}$). Usually data were recorded for two runs at each speed. Each run was at a constant speed on an even surface, which has both advantages and disadvantages. The main advantage is that we could determine the effects of both speed and gait on strain patterns. The main disadvantage is that we missed the effects of acceleration and deceleration and of running on uneven surfaces, which are likely to load the hoof in quantitatively different ways in comparison with locomotion at constant speed.

The strain gauges were energized as one-quarter of a Wheatstone bridge by strain-conditioning amplifiers (model 2120, Measurements Group, Inc., Raleigh, North Carolina, USA). The amplifier output represents strain as d.c. voltage with a high-frequency cut-off at 5 kHz. Strain signals were digitally sampled, usually at 300–500 Hz, and entered directly into a microcomputer to calculate principal strains and directions (using formulae from Dally and Riley, 1965). We attempted to record 10 or more strides per speed, achieving this in most cases (see Table 1: *N*). Strain directions were calculated with respect to the tubules and intertubular material to the nearest 5°. As principal stresses could not be calculated, because shear moduli have not been determined for hoof material, we estimated safety factors on the basis of strain rather than stress, using the strains at material failure reported by Bertram and Gosline (1986).

Rates of change of strain were calculated for the three highest speeds, which were all sampled at 500 Hz. We also subjected single strides from each of these runs to a Fast Fourier Transform (adding zeros as necessary to give 512 values for analysis). We report the range of frequencies constituting 95 % of the resulting power spectrum. (The highest such frequency is less than half the sampling rate and should, therefore, have been accurately sampled.) The rationale for these calculations is that the strength and stiffness of most materials is dependent upon strain rate. All the *in vitro* materials tests we have described were essentially static. The values we report of *in vivo* strain rates and biologically relevant loading frequencies will allow future workers to examine time dependence *in vitro*.

Results

Each gauge site showed repeatable patterns of strain among strides at any speed. Fig. 3 shows the principal strains determined for each gauge on pony 1 during five strides of a trot at 3 $m\,s^{-1}$. The major changes with speed and gait are in

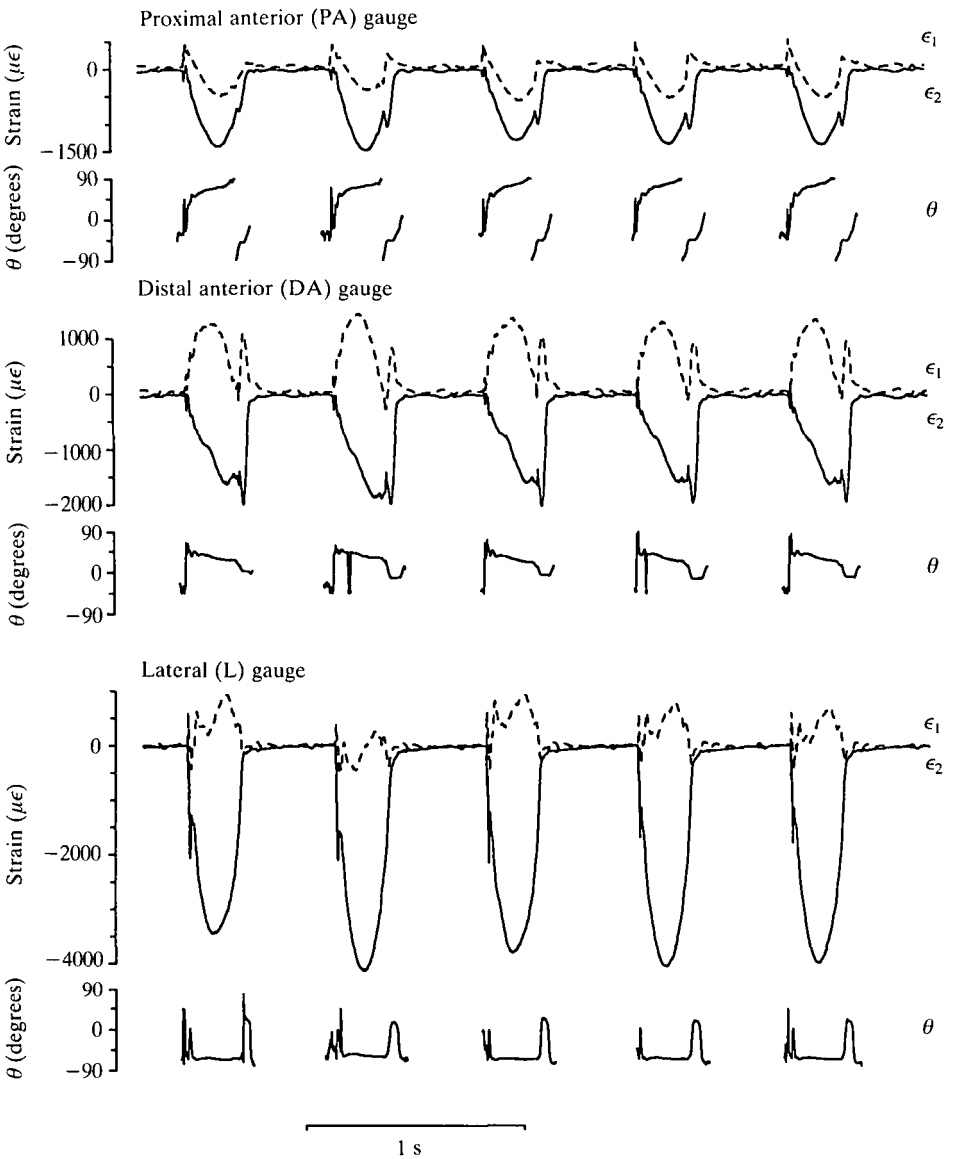

Fig. 3. Representative principal strain records (ϵ_1, tensile, and ϵ_2, compressive, in microstrain, $\mu\epsilon$) from all three gauges on pony 1 during five strides of a trot at 3 m s^{-1}. Angle θ (in degrees) is calculated from the tubular axis to principal strain ϵ_2; positive is anticlockwise. As +90° and −90° are the same orientation, some lines disappear off the top of the graph and reappear at the bottom. When the hoof is off the ground, the angles are noisy, because the strains are near zero, and have been omitted.

strain magnitude and duration of the stance phase, and not in the general shape of the records. The position of transient spikes and the orientation of the principal strains to the tubules are largely unaffected by speed or gait. Fig. 4 shows

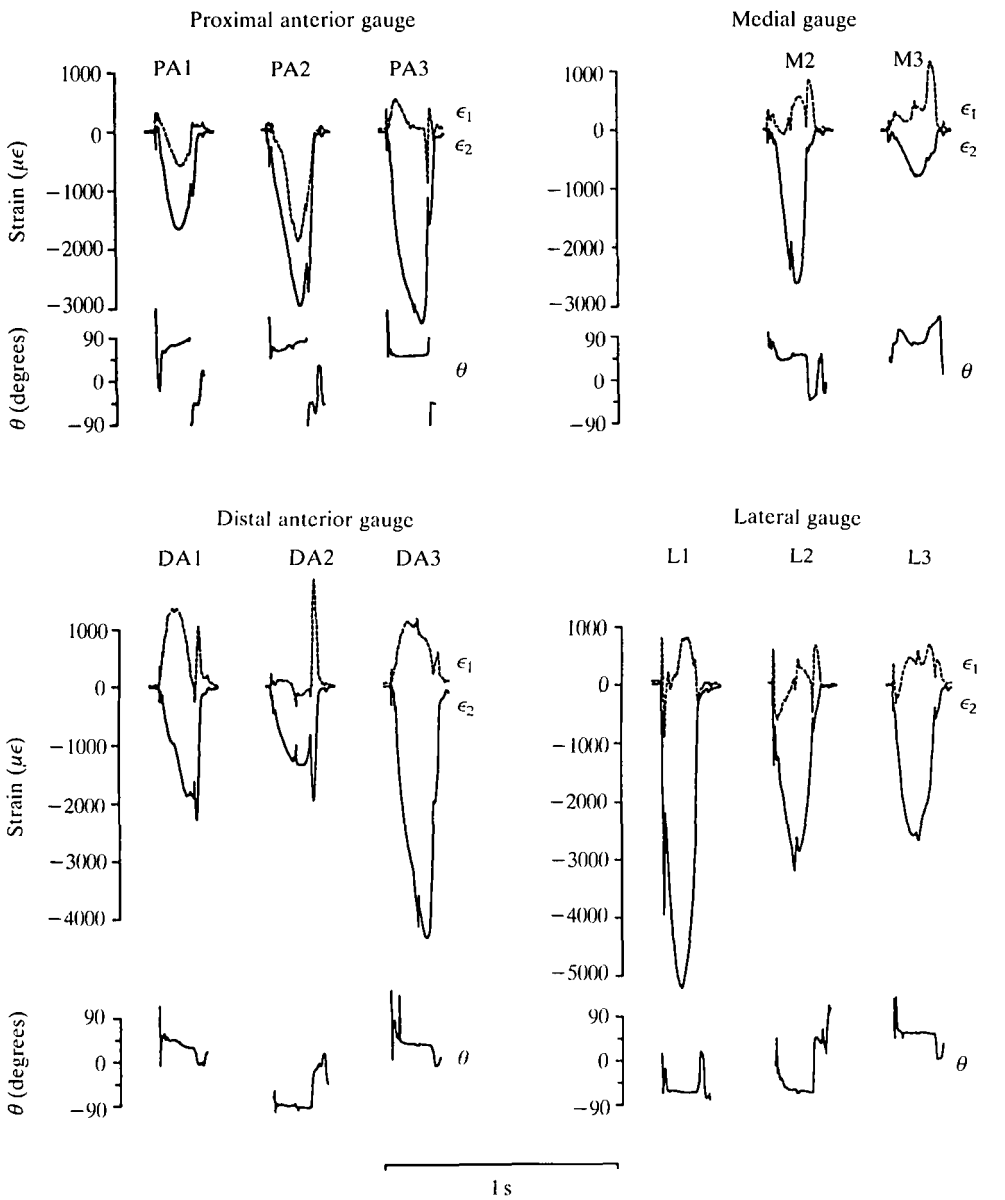

Fig. 4. Representative principal strain records from all gauge sites on all three animals during one stride of a trot at 3.75 m s^{-1}. PA, DA, L and M refer to the gauge sites; postfixed numbers are the animal codes. Further description as in Fig. 3.

representative records of principal strain for all gauge sites on all three animals for one stride at a 3.75 m s^{-1} trot. Comparable plots for strides at other speeds would have a similar appearance.

The compressive principal strain (ϵ_2) is generally larger than the tensile

principal strain (ϵ_1), indicating the predominantly compressive loading of the wall. Several sites show evidence of biaxial compression. The proximal anterior (PA) gauge of all three animals is loaded in biaxial compression at the midpoint of the stance phase of all gaits and speeds. This is most obvious for ponies 1 and 2: principal strains ϵ_1 and ϵ_2 are both in compression at mid-stance phase, when ϵ_2 is at its peak (Fig. 4: PA1, PA2). (Compare PA and DA traces in Fig. 3. The DA gauge shows the more common result of tensile ϵ_1 and a larger compressive ϵ_2 at mid-stance phase, indicating compression essentially in one direction.) In pony 3, ϵ_1 is near zero at mid-stance phase (Fig. 4: PA3). This also indicates biaxial compression: ϵ_1 would normally be a tensile strain as the material tended to retain its volume while being compressed in the direction of ϵ_2. However, the tension is cancelled by compressive loading. Such cancellation is also seen in gauge DA2. The low ratio of ϵ_1 to ϵ_2 at mid-stance phase in all lateral and medial gauges is also suggestive of unequal biaxial compression, with partial cancellation of the tensile ϵ_1. Without knowing Poisson's ratios for the material at these locations, it is difficult to be certain.

The orientation of peak principal strains, at mid-stance phase, does not consistently correspond with tubular (θ_T) or intertubular (θ_I) axes in the hoof material (Table 1, Fig. 5). The largest principal strain (ϵ_2) is oriented more than 25° from either material axis in seven of the eleven gauges. Correspondence is better for the other four gauges (PA1, PA2, DA2, M3) for which peak ϵ_2 (compression) is within 0–20° of the intertubular material (Table 1: θ_I). For the three anterior gauges in this list, peak ϵ_1 (also compression) has the same small range of divergence from the tubules, because tubules and intertubular material are orthogonal at the toe. The orientation of these strains at mid-stance phase is largely unaffected by speed or gait (Table 1). Changes of 10° or less are predominant, and the maximum is 20° (for PA1 and PA2).

The magnitude of peak principal strain ϵ_2 at any gauge site is quite repeatable among strides at any speed. The standard deviations in Table 1 are between 2 and 15% of the corresponding means. The magnitude of ϵ_2 generally increases, somewhat irregularly, with speed (Fig. 6), the irregularity probably due in great part to changes in gait. All lateral gauges show a drop in peak ϵ_2 at the trot–canter transition, as does gauge DA2. (All the animals used the leg with the gauges as the non-lead leg at the canter; it contacted the ground before the other forelimb in each stride.) Gauges PA1 and DA1 are unusual in showing a small decrease in the magnitude of ϵ_2 between canters at 4.5 and 6.0 $m\,s^{-1}$. Peak strains of greater magnitude than $-3000\,\mu\epsilon$ (microstrain) are common at the fastest speed, with the maximum recorded being $-4863\,\mu\epsilon$ for DA3 at 6.0 $m\,s^{-1}$. The largest changes in strain with speed occur at the lateral gauges, averaging $2050\,\mu\epsilon$, compared with averages for the other gauges of: PA, $1180\,\mu\epsilon$; DA, $950\,\mu\epsilon$; and M, $770\,\mu\epsilon$.

All the strain traces show transient spikes superimposed on the generally sinusoidal rise and fall of ϵ_2 during the stance (Fig. 4). There is usually a small spike at impact (much larger on L1) and another spike towards the end of the stance, particularly at PA and DA gauges. This spike occurs at breakover (when

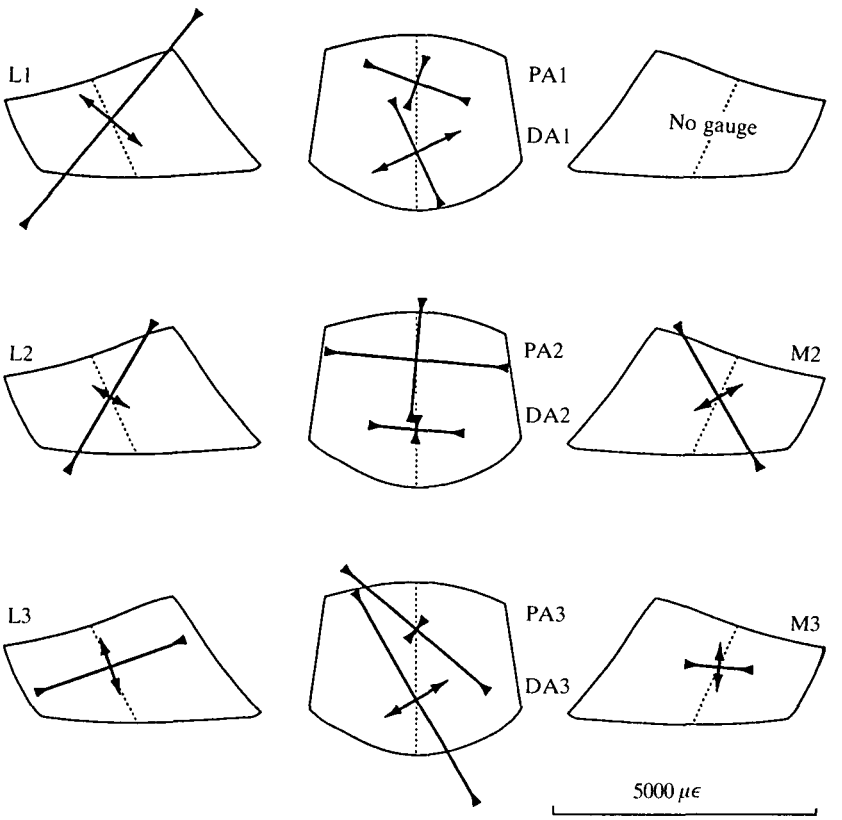

Fig. 5. Stylized sketches of lateral, anterior and medial views of horse hooves showing the mean magnitudes and orientations of peak principal strains ϵ_1 and ϵ_2 from all gauge sites at a 3.75 m s^{-1} trot (data from Table 1). Strain orientations are drawn with respect to the dotted lines representing local alignment of the tubules. Orientation of the intertubular material has been omitted for clarity, but Table 1 shows that strains are generally not well aligned with this material.

the hoof rolls onto the toe to push off at the end of the stance phase) and represents a change in loading pattern at all the gauge sites. Strain orientations, which are steady or slowly changing through most of the stance phase, change rapidly at the onset of this spike (Fig. 4). On the anterior gauges, magnitudes of ϵ_2 are still sizable, 45–90 % of peak. But only PA2 shows strong biaxial compression, and ϵ_2 on the distal gauges is now closely aligned with the tubules (Fig. 7). The tensile ϵ_1 is aligned with the intertubular material. On the lateral and medial gauges, strains are small, but tension (ϵ_1) equals or exceeds compression (ϵ_2) in most cases (Fig. 4).

Strain rates vary between 0.02×10^6 and 1.7×10^6 $\mu\epsilon$ s^{-1}. The largest value is for the impact spike on gauge L1; the spikes at breakover have rates of the order of 0.25×10^6 $\mu\epsilon$ s^{-1}, and the smallest values are for the smooth rise towards peak strain at mid-stance phase. In the Fourier analysis of individual strides at the faster

Table 1. *Mean magnitudes and standard deviations for peak principal compressive strain (ϵ_2, in microstrain) for all running speeds (in $m\,s^{-1}$)*

	Proximal anterior gauge														
	PA1					PA2					PA3				
Speed	Strain	S.D.	θ_T (degrees)	θ_I (degrees)	N	Strain	S.D.	θ_T (degrees)	θ_I (degrees)	N	Strain	S.D.	θ_T (degrees)	θ_I (degrees)	N
1	−830*	159.2	70	−20	13	−1862*	70.0	85	−5	9	−2570*	97.3	50	−40	8
1.5	−1062*	85.3	80	−10	4	−2290*	82.2	80	−10	11	−2850	188.1	50	−40	10
2	−1218*	73.9	70	−20	12	−1850*	185.1	90	0	11	−2783*	78.9	50	−40	13
3	−1383*	45.1	70	−20	9	−2726*	68.1	70	−20	22	−3029	68.7	55	−35	11
3.75	−1628*	38.7	75	−15	10	−2993*	46.8	85	−5	9	−3106*	64.8	55	−35	12
4.5	−1625*	87.3	90	0	11	−3172*	90.4	80	−10	12	−3441*	82.3	55	−35	12
6	−1500*	231.4	90	0	5	−3674*	62.1	75	−15	22	−3504*	80.6	50	−40	12

	Distal anterior gauge											
	DA1				DA2				DA3			
Speed	Strain	S.D.	θ_T (degrees)	θ_I (degrees)	Strain	S.D.	θ_T (degrees)	θ_I (degrees)	Strain	S.D.	θ_T (degrees)	θ_I (degrees)
1	−1127	157.4	25	−65	−790*	37.0	85	−5	−3590	127.5	30	−70
1.5	−1368	177.0	25	−65	−899*	59.1	85	−5	−3751	393.1	30	−70
2	−1412	262.8	30	−60	−837*	76.2	85	−5	−3613	103.4	30	−70
3	−1634	95.3	30	−60	−1178*	58.9	90	0	−3997	104.7	30	−70
3.75	−1743	91.7	25	−65	−1333*	55.2	85	−5	−4176	121.9	30	−70
4.5	−1838	181.0	30	−60	−1260*	43.3	85	−5	−4722	136.1	30	−70
6	−1197	402.1	30	−60	−1657*	92.3	90	0	−4863	155.5	30	−70

Table 1. *Continued*

	Lateral gauge											
	L1				L2				L3			
Speed	Strain	S.D.	θ_T (degrees)	θ_l (degrees)	Strain	S.D.	θ_T (degrees)	θ_l (degrees)	Strain	S.D.	θ_T (degrees)	θ_l (degrees)
1	−1861	297.8	−75	35	−901	125.8	−60	50	−953	45.3	80	30
1.5	−1920	315.8	−75	35	−1240	204.5	−60	50	−1328	228.9	80	30
2	−2710	272.3	−70	40	−1866	343.0	−65	45	−1599	78.5	85	25
3	−3801	294.5	−75	35	−2507	330.2	−60	50	−2108	86.7	85	25
3.75	−4724	299.4	−85	25	−2805	254.2	−60	50	−2487	108.2	85	25
4.5	−2785	244.1	−75	35	−2170	394.2	−65	45	−2407	198.8	90	20
6	−3662	828.0	−80	30	−3191	373.9	−55	50	−3049	122.9	90	20

		Medial gauge							
		M2				M3			
Speed	M1 No medial gauge	Strain	S.D.	θ_T (degrees)	θ_l (degrees)	Strain	S.D.	θ_T (degrees)	θ_l (degrees)
1		−1865	284.1	60	−40	−594*	85.0	−75	−5
1.5		−2540	303.0	55	−45	−596	135.7	−75	−5
2		−1746	412.1	55	−45	−710	91.4	−75	−5
3		−2406	332.9	60	−40	−779	62.0	−75	−5
3.75		−2697	178.1	60	−40	−806	67.9	−75	−5
4.5		−2844	306.1	60	−40	−1163	231.3	90	−20
6		−3319	393.7	65	−35	−1455	163.4	90	−20

All gauge sites on each animal are shown.
The mean orientation of ϵ_2 with respect to the tubules (θ_T) and intertubular material (θ_l) at each site is given in degrees.
N is the number of strides averaged at each speed.
Asterisks identify where peak ● was also compressive.

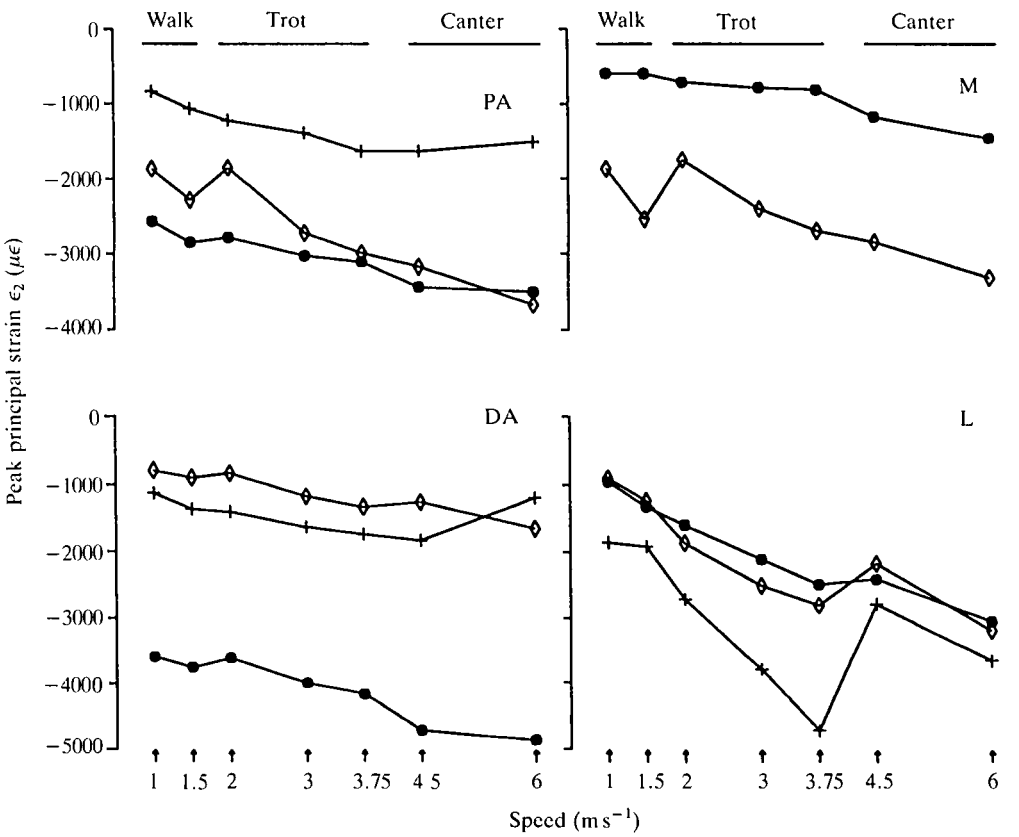

Fig. 6. Graphs of peak principal strain ϵ_2 against speed and gait for all gauge sites (data from Table 1). Crosses, pony 1; open diamonds, pony 2; filled circles, pony 3.

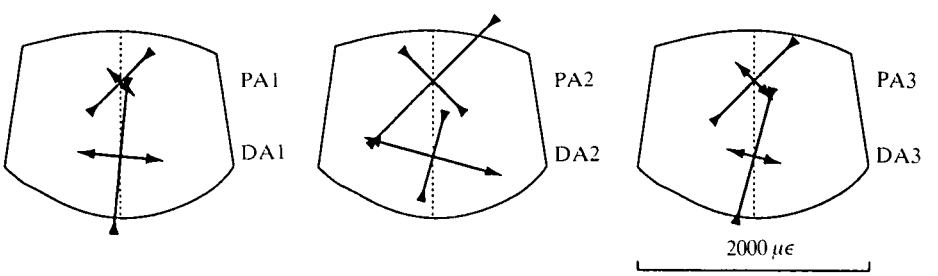

Fig. 7. Mean magnitudes and orientations of principal strains ϵ_1 and ϵ_2 at the peak of the push-off spike for all anterior gauges at a 3.75 m s^{-1} trot. Note the change in scale from Fig. 5. Strains on the L and M gauges were low at this point in the step and were not included.

speeds, we looked for the upper frequency bounding 95 % of the power spectrum. The highest such frequency was 216 Hz, with most falling between 90 Hz and 180 Hz, varying among gauge sites and individuals.

Discussion

The material at each gauge site is loaded with two different patterns of strain during the stance phase. For most of the stance, the magnitude of the largest principal strain (ϵ_2) rises then falls, following the magnitude of the vertical component of the ground reaction force on the hoof (Biewener *et al.* 1983). Strain orientation varies slowly, if at all, during this time. Compression is predominant at all sites and is biaxial at the PA site, which helps resist fracture of the material: cracks will tend to be closed rather than opened. Furthermore, biaxial compression actually lowers peak strain levels because the compressive strain in each direction is reduced by the principal tensile strain perpendicular to the other direction.

The second pattern occurs at breakover when there is a sudden increase in strain levels, which had been dropping. Strain orientation swings rapidly and markedly on the anterior gauges, while tension may become predominant on the lateral and medial gauges. At this point in the stance phase the heels have been lifted from the ground, and absolute load levels are decreasing rapidly (Biewener *et al.* 1983). The large proximodistally oriented compressive spike indicates dorsiflexion of the wall at the toe, as the hoof 'rolls over', and this region bears all the remaining load.

The two patterns are consistent at each site over the range of gaits and speeds studied. (There is some individual variation, but that is to be expected, given the variation in hoof shape among the animals.) The magnitudes of peak principal strains ϵ_2 increase predictably with speed, corresponding to an increase in the ground reaction force (Biewener *et al.* 1983), with some variability owing to changes in gait. Strain orientation at any point during the stance phase is affected little, if at all, by speed or gait.

At the midpoint of the stance phase, peak principal strain ϵ_2 shows regular changes in orientation with respect to the tubules around the circumference of the hoof. This is most clear in pony 2 (Fig. 5), in which the orientation of the larger principal strain ϵ_2 rotates from being $-60°$ with respect to the tubules on the lateral gauge L2, to being nearly perpendicular to the tubules (and close to horizontal) at PA2, to having an orientation of $+60°$ at medial gauge M2. If the inclination of ϵ_2 changes as smoothly as it appears, it would be exactly aligned with the intertubular material slightly lateral to the position of the PA gauge. We might consider this a functional axis, distinct from the morphological axis of the hoof. The change in orientation is not as regular for pony 3; there may be places on either side of the midline where ϵ_2 is aligned with the intertubular material. The relatively low magnitude of strain on gauge M3 and its orientation suggest that it is primarily due to heel spreading rather than to weight-bearing. The functional axis of this hoof is, therefore, likely to be between the anatomical midline and the lateral gauge site. Certainly pony 3 does not load the medial wall of its hoof to the same extent as does pony 2. While the patterns on any one hoof are consistent, they are individually variable, which probably results, in part, from the differences in shape and asymmetry of the hooves among the animals. The symmetrical

distribution of strain in pony 2 suggests that this animal had the most balanced distribution of load between the lateral and medial quarters of its hoof.

Loading and distortion of the hoof wall

The hoof of each animal appears to be distorted in a regular repeatable manner during the stance phase. Of course, we ran the animals at constant speeds on a flat, moderately compliant substratum (a rubber treadmill belt moving over a fixed metal plate). Irregular substrata will cause local distortions and increases in stress superimposed over these repeatable patterns. We discuss these in relation to material properties below. Furthermore, cornering, acceleration, deceleration and jumping will change the manner of distortion, as will shoeing. However, it is likely that each will superimpose its own pattern of distortion over the general pattern we observed. For example, shoeing, which probably stiffens the hoof markedly, does not prevent heel spreading (Colles, 1989*b*) or biaxial compression of the material at the toe (J. J. Thomason, A. P. Russell and S. Hunt, unpublished results).

The strain patterns we recorded accord well with the models of hoof-wall loading described in the Introduction. The predominance of compressive peak principal strains fits with the wall's role of transmitting forces of weight-bearing between the skeleton and the ground. The off-axis orientation of the peak principal strains and the biaxial compression at the toe both correlate with the concept of three-dimensional distortion of the wall and spreading of the heels.

Strains recorded at the quarters show that heel spreading does not occur simply in the horizontal plane (as suggested in Fig. 2D). The lateral gauges, in particular, indicate that the lower margin of the heels may be spread further than their more proximal edge. The strain orientations give the impression that the lower edge of the heel is being 'rolled' out and up towards the coronary border at the toe. This interpretation corresponds with the combined loading situations in Fig. 2C and D. Other interpretations are possible; it would be necessary to have gauges on the inner surface of the wall to be sure, and we have already noted the undesirability of doing that. It is, however, almost certain that spreading of the heels is affecting the strain pattern at the quarters. This is important for interpreting the biaxial compression at the toe.

The more vertically oriented compressive strain at the toe is likely to be due to weight transmission through the wall (Fig. 2A). The more horizontal one is probably from distortion of the hoof. It is interesting that the horizontal strain is larger on gauges PA1 and PA2. While heel spreading is an obvious probable cause for the horizontal compression, we suggest that a larger contribution to this strain comes from the inwardly directed forces suspending P_{III}. Fig. 8 shows how these radial forces might cause tangential compression at the surface by flattening the curvature at the toe. Certainly the anterior wall of the hoof does move posteriorly (as seen in sagittal radiographs) in response to the tension between the *stratum internum* and P_{III} (Fischerleitner, 1974), and the anterior half of the coronary border becomes constricted (Lungwitz, 1891, cited in Colles, 1989*a*). For several

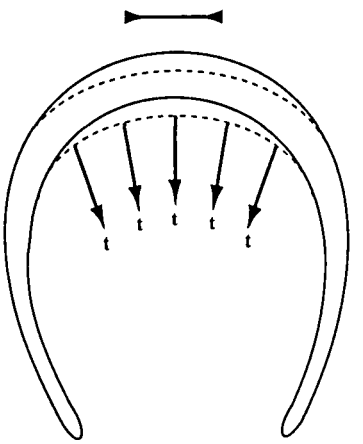

Fig. 8. Diagrammatic horizontal section through the hoof wall and lamellar junction. The inwardly directed forces (**t**) on the wall from P_{III} (*via* the lamellar junction) probably increase the radius of curvature at the toe and induce tangentially oriented compressive strain.

reasons, we favour this explanation as a more important contributor to the biaxial compression than heel spreading. First, only gauge DA2 shows biaxial compression at peak loading (Fig. 5). Heel spreading should induce horizontal compression at the DA site as well as at the PA site. We might even expect more horizontal strain at the distal site because the material is towards the lower margin of the lamellar junction binding it to P_{III}. The attachment of the distal part of the wall to the sole is probably less constraining on distortion than is the lamellar junction. Second, biaxial compression may still exist at breakover when the heels are no longer in contact with the ground. Strains on the quarters are much lower at this time yet gauge PA2 is still in biaxial compression, and the low tensile strain ϵ_1 on PA1 suggests it may be partly cancelled by tensile strains perpendicular to the horizontal compression. Third, shoeing does not diminish the biaxial compression. The heels of a shod horse are still free to expand and do so (Colles, 1989*a*). However, the quarters and toe should be firmly nailed to the shoe, which is considerably stiffer than the hoof wall and, therefore, likely to impede the quarters from also spreading. Yet the relative magnitudes of vertical and horizontal strains at the toe (recorded from single foil gauges) are the same with or without shoes on the same animal (J. J. Thomason, A. P. Russell and S. Hunt, unpublished results). Finally, as we observed in the Introduction, the walls are considerably thinner and more pliant at the heels than elsewhere in the hoof and are capable of being deformed locally without greatly affecting the rest of the wall.

Functional design of the stratum medium

Given the consistency of strain patterns, particularly in their orientation, we were initially surprised that peak principal strains are generally not well aligned

with the material axes (Table 1, Figs 5, 7). The changes in strain orientation around the circumference emphasize that the material is loaded along its microscopic axes primarily at the functional axis of the hoof. The microarchitecture of hoof wall is clearly an adaptation to mechanical function and we expected better general alignment of peak strains with the material axes. We were perhaps distracted by the strong resemblance to some man-made composites, such as a unidirectional fibreglass. This material is strongest and stiffest in the fibre direction, and the function of the matrix between the fibres is to absorb energy and prevent cracks from spreading from one fibre to another (Harris, 1980). However, the mechanical studies reviewed in the Introduction demonstrate that hoof material is not simply fibre (tubules) and matrix (intertubular material). The intertubular material is itself reinforced by keratin fibrils and contributes more to the strength, stiffness and fracture toughness than do the tubules. Tensile and compressive stiffness are both greater in the intertubular direction, while the tubules are three times more likely to fracture (Leach, 1980; Bertram and Gosline, 1986).

Our results dovetail well with the concept of the *stratum medium* as a multidirectional composite. Leach (1980) was puzzled when he found that the material was stiffer in a direction perpendicular to the way in which he thought it was loaded. This problem is now resolved: the principal strains are mostly not aligned with either of the material directions. The organization of the material makes it sufficiently strong, stiff and tough in all directions for the orientation of the peak principal strains it normally experiences to be immaterial. It also absorbs energy well, which is important in resisting impact of the hoof with the ground. These assertions are supported by comparing the magnitudes of peak principal strain *in vivo*, and calculated values of energy absorbed by the material, with the maxima that the material can tolerate. The comparisons below are based on the assumption that peak principal compressive strains are aligned with the stiffer intertubular axis. Our results show this need not be the case, but the anisotropy in material properties is small enough not to invalidate the arguments. We also confine the discussion to compression in the plane of the surface. These strains result from overall bending of the hoof wall and may, therefore, be accompanied by tangential tensile strains at the deep border of the *stratum medium*. The arguments hold for such tensile strains. We have no basis for discussing radially directed strains.

Energy-absorbing materials can generally tolerate high strains (Wainwright *et al.* 1976). The largest principal compressive strains were approximately $-5000\,\mu\epsilon$, compared with maximal strains of $-2800\,\mu\epsilon$ in the radius and $-3200\,\mu\epsilon$ in the tibia of galloping horses (Rubin and Lanyon, 1982), that is under similar locomotory conditions to those provided at the fastest speeds in our experiment. The horses we used were small (170 kg). Records from single-element gauges on the hooves of larger animals (400 kg) reached $-5000\,\mu\epsilon$ at a medium trot or slow canter on concrete (J. J. Thomason, A. P. Russell and S. Hunt, unpublished results). Peak strains in the hooves of large horses at a fast gallop on hard ground

probably approach or exceed $-6000\,\mu\epsilon$ (excluding excessive local strains at the free margin caused by impact with stones, etc.). The material yields in tension at $25\,000\,\mu\epsilon$ (at 75% relative hydration) and then has a long plastic region before failing at $150\,000\,\mu\epsilon$ or 15% strain (Bertram and Gosline, 1987). Assuming the compressive yield strain (which has not been reported) to be approximately the same for that in tension, the safety factor between operating and yield strains is roughly 4–5. This compares with a range of 2–5 for locomotory stresses at high speed in the long limb bones of mammals of different sizes (Biewener, 1989).

Another property common to many energy-absorbing materials is a low to moderate stiffness or elastic modulus (Wainwright *et al.* 1976). The tensile and compressive elastic moduli of hoof keratin range from 0.4 to 0.6 GPa in the intertubular direction (Leach, 1980; Bertram and Gosline, 1986), which is an order of magnitude less than the values for most keratinous tissues studied (Fraser and MacRae, 1980). For comparison, elastic moduli for bone are 7–27 GPa (Currey, 1984). The peak principal strains we obtained fall in the linearly elastic range for hoof wall keratin, and compressive strain energy may be calculated from peak strain ϵ and the elastic modulus E as $\frac{1}{2}(\epsilon^2 E)$. Taking ϵ to be $-5000\,\mu\epsilon$ and E to be 0.5 GPa gives a value of 6.25 kJ m^{-3}. The total strain energy capacity before failure for keratin is three orders of magnitude greater (Wainwright *et al.* 1976). Perhaps a more appropriate comparison is with the strain energy absorbed before elastic yield. Bertram and Gosline's (1987) tensile experiments give a value of 62.5 kJ m^{-3} for material at 75% relative humidity (working from their Fig. 4, p. 127). Assuming again that the compressive value is reasonably close to that for tension, the *stratum medium* absorbs energy to one-tenth of its yield capacity during normal locomotion.

We can now summarise the functional design of the *stratum medium*. The strong orientation of the microarchitecture affects the anisotropy of different mechanical properties in different ways. Strength and stiffness are weakly or moderately anisotropic, by amounts that appear to be functionally unimportant. What is important is that the material is capable of withstanding strains in any orientation, and this ability is definitely a function of its construction. Tubules or intertubular material alone would be markedly weaker perpendicular to their orientation. In contrast, the anisotropy in toughness has profound functional consequences. Because it is higher in the tubular direction, cracks will propagate, if at all, perpendicular to the free margin of the hoof. They are very unlikely to extend towards the lamellar junction in a healthy hoof (though such cracks do occur in extremely dry hooves, as an effect of the low hydration, and also in the largest breeds of horse, perhaps as a size-related effect). Again it is the composite nature of the material that gives these crack-diverting properties, though the compressive loading at the surface helps close cracks.

Comparison of hoof keratin with bone

The design characteristics of the hoof wall may be compared with those of bone, whose functional adaptations have been well studied (and reviewed by Currey,

1984). Hoof keratin is not a living tissue and cannot remodel in response to operating strains as can bone. Comparison of the output from PA and DA gauges shows that the orientation of peak principal strains may, in fact, change as the tubules migrate. Certainly the peak principal strains at mid-stance phase are not at the same orientation as those of the spike at breakover. Hoof material has to be able to tolerate changes in loading regime as it migrates down the wall and during any given stride. Its particular form of composite construction allows it to be stressed in any direction. This contrasts with Haversian bone, which has a definite 'grain', anatomically and mechanically (Currey, 1984).

The change in properties near the distal margin of the hoof, where tensile strength increases while fracture toughness reduces, is accomplished by the response of the material to hydration gradients within it (Bertram and Gosline, 1987). Similarly, the increased compliance of the deeper levels of *stratum medium* and of the *stratum internum*, which is partly dependent on a high level of hydration, protects the living cells of the dermis from shock. No comparable strategies based on hydration level are apparent in bone. While drying does affect the properties of bone, such conditions do not normally occur. In life it is fully hydrated (antlers being an obvious exception).

Loading of the hoof wall is likely to be less predictable than in most bones because the animal has no control over irregularities in the substratum. The crack-diverting properties of the material are certainly a defence against unpredictable loading. In contrast, some bones have a mechanism for making loading regimes more predictable (Bertram and Biewener, 1988). The curvature of long limb bones ensures that, under normal operating conditions, they will be bent in a consistent direction. While tending to increase stress magnitudes, this mechanism guarantees predictability of stress patterns in the bone material at any point on the diaphysis.

Future directions

This study has gone some way towards linking *in vitro* material testing of the hoof wall with its manner of loading *in vivo*. To continue this line of research more information is needed on the material properties of the hoof wall. Poisson's ratios and shear moduli are necessary for calculation of principal stresses as well as for evaluating the relative magnitudes of the biaxially compressive strains on the anterior wall. Given that the material is loaded in compression at the surface, compressive strains and stresses at yield and failure should be assessed (Leach, 1980, reported forces at compressive yield for standard-sized specimens, from which yield stresses could be calculated). The great difference in magnitude between peak ϵ_1 and peak ϵ_2 at many gauge sites indicates a high degree of shear in the material. Shear strains can be easily calculated from ϵ_1 and ϵ_2, but the exercise is meaningless in the absence of information on how the material behaves under shear loading.

While strain gauges have been used quite extensively on the hoof wall, there is still useful information to be obtained from them. We only investigated four sites. Given the complex manner in which the hoof deforms, a more complete picture

could be obtained by using more rosette gauges. The effects of cornering, acceleration, deceleration and irregular substrata, factors we deliberately avoided in this study, could be addressed. Even the effects of shoeing are not yet completely understood.

Once the material properties and surface strain patterns are more completely documented, finite element analysis provides the means of modelling patterns of stress and strain throughout the whole hoof, not just the wall. The deceptively simple exterior of the hoof conceals a suite of structural adaptations contributing to the locomotory specialization of the limb. The functions of the digital pad, lateral cartilages and frog, for example, are incompletely understood. The present study advances our understanding of the adaptations in the hoof wall while, literally and figuratively, only scratching the surface.

We thank Dr C. R. Taylor for use of the treadmill, research animals and facilities at the Concord Field Station, Harvard University; Claire Farley and Roger Kram for their expert assistance with the animals; Jean-Michel and Charlotte Weber for their hospitality; Danette Pratt for preparing Figs 2, 5, 7 and 8; and three reviewers for their constructive comments. This work was supported by funding from the Ohio University College of Osteopathic Medicine to J.J.T. and by NSF grant DCB 9019767 to A.A.B.

References

BARTEL, D. L., SCHRYVER, H. F., LOWE, J. E. AND PARKER, R. A. (1978). Locomotion in the horse: a procedure for computing the internal forces in the digit. *Am. J. vet. Res.* **39**, 1721–1727.

BERTRAM, J. E. A. AND BIEWENER, A. A. (1988). Bone curvature: sacrificing strength for load predictability? *J. theor. Biol.* **131**, 75–92.

BERTRAM, J. E. A. AND GOSLINE, J. M. (1986). Fracture toughness design in horse hoof keratin. *J. exp. Biol.* **125**, 29–47.

BERTRAM, J. E. A. AND GOSLINE, J. M. (1987). Functional design of horse hoof keratin: the modulation of mechanical properties through hydration effects. *J. exp. Biol.* **130**, 121–136.

BIEWENER, A. A. (1989). Scaling body support in mammals: limb posture and muscle mechanics. *Science* **245**, 45–48.

BIEWENER, A. A., THOMASON, J. J., GOODSHIP, A. AND LANYON, L. E. (1983). Bone stress in the horse forelimb during locomotion at different gaits: a comparison of two experimental methods. *J. Biomech.* **16**, 565–576.

CARTER, D. R. (1978). Anisotropic analysis of strain rosette information from cortical bone. *J. Biomech.* **11**, 199–202.

COFFMAN, J. R., JOHNSON, J. H., FINOCCHIO, E. J. AND GUFFY, M. M. (1970). Biomechanics of pedal rotation in equine laminitis. *J. Am. vet. med. Ass.* **156**, 219–221.

COLLES, G. M. (1989*a*). The relationship of frog pressure to heel expansion. *Eq. vet. J.* **21**, 13–16.

COLLES, G. M. (1989*b*). A technique for assessing hoof function in the horse. *Eq. vet. J.* **21**, 17–22.

CURREY, J. D. (1984). *The Mechanical Adaptations of Bones.* Princeton, NJ: Princeton University Press.

DALLY, J. W. AND RILEY, W. F. (1965). *Experimental Stress Analysis.* New York: McGraw-Hill.

FISCHERLEITNER, F. (1974). Röntgenographische Untersuchungen über den Einfluss der Lageveranderungen des Huf-Strahl und Kronbeines auf die Mechanik der Hornkapsel des Pferdes im Belastungsgerat. Inaugural dissertation, Vienna.

FRASER, R. D. B. AND MACRAE, T. P. (1980). Molecular structure and mechanical properties of keratins. In *The Mechanical Properties of Biological Materials. Symp. Soc. exp. Biol.* XXXIV (ed. J. F. V. Vincent and J. D. Currey), pp. 211–246.

GETTY, R. (1975). *Sisson and Grossman's The Anatomy of the Domestic Animals*, vol. 1. Philadelphia, PA: Saunders.

HARRIS, B. (1980). The mechanical behaviour of composites. In *The Mechanical Properties of Biological Materials. Symp. Soc. exp. Biol.* XXXIV (ed. J. F. V. Vincent and J. D. Currey), pp. 37–74.

KNEZEVIC, P. F. (1962). Klinik des Trachtenzwanghufes und Grundlagen der Ungulographie mit Dehnungsmeßstreifen beim Pferde. *Wien. tierärtzl. Monatsschr.* **49**, 777–824, 869–904, 944–959.

LEACH, D. H. (1980). The structure and function of equine hoof wall. PhD thesis, Department of Veterinary Anatomy, University of Saskatchewan, Saskatoon, Saskatchewan, Canada.

LEACH, D. H. AND OLIPHANT, L. W. (1984). Degradation of annular gap junctions of the equine hoof wall. *Acta anat.* **120**, 214–231.

MAIR, F.-J. (1974). Dehnungsmessungen an der Hornwand in Tragrandnähe und der Hornsohle beim Pferd-Hinterhuf. *Wien. tierärtzl. Monatsschr.* **61**, 70–71.

PREUSCHOFT, H. (1989). The external forces and internal stresses in the feet of dressage and jumping horses. *Z. Saugetierkunde* **54**, 172–190.

RUBIN, C. T. AND LANYON, L. E. (1982). Limb mechanics as a a function of speed and gait: a study of functional strains in the radius and tibia of horse and dog. *J. exp. Biol.* **101**, 187–211.

STUMP, J. E. (1967). Anatomy of the normal equine foot, including microscopic features of the laminar region. *J. Am. vet. med. Ass.* **151**, 1588–1599.

WAINWRIGHT, S. A, BIGGS, W. D, CURREY, J. D. AND GOSLINE, J. M. (1976). *Mechanical Design in Organisms*. London: Edward Arnold.

ZOERB, G. C. AND LEACH, D. H. (1978). The mechanical properties of the hoof wall of the horse. *Am. Soc. agric. Eng., Tech. paper* 78–3063.